ResearchGate

See discussions, stats, and author profiles for this publication at: https://www.researchgate.net/publication/50935223

Quantum Master Equation Method Based on the Broken-Symmetry Time-Dependent Density Functional Theory: Application to Dynamic Polarizability of Open-Shell Molecular Systems

ARTICLE *in* THE JOURNAL OF PHYSICAL CHEMISTRY A · MARCH 2011

Impact Factor: 2.69 · DOI: 10.1021/jp200056m · Source: PubMed

CITATIONS
7

READS
21

2 AUTHORS:

Ryohei Kishi
Osaka University
110 PUBLICATIONS **1,940** CITATIONS
SEE PROFILE

Masayoshi Nakano
Osaka University
337 PUBLICATIONS **4,769** CITATIONS
SEE PROFILE

Available from: Masayoshi Nakano
Retrieved on: 24 January 2016

THE JOURNAL OF PHYSICAL CHEMISTRY A

ARTICLE

pubs.acs.org/JPCA

Quantum Master Equation Method Based on the Broken-Symmetry Time-Dependent Density Functional Theory: Application to Dynamic Polarizability of Open-Shell Molecular Systems

Ryohei Kishi* and Masayoshi Nakano*

Department of Materials Engineering Science, Graduate School of Engineering Science, Osaka University, Toyonaka, Osaka 560-8531, Japan

ABSTRACT: A novel method for the calculation of the dynamic polarizability (α) of open-shell molecular systems is developed based on the quantum master equation combined with the broken-symmetry (BS) time-dependent density functional theory within the Tamm-Dancoff approximation, referred to as the BS-DFTQME method. We investigate the dynamic α density distribution obtained from BS-DFTQME calculations in order to analyze the spatial contributions of electrons to the field-induced polarization and clarify the contributions of the frontier orbital pair to α and its density. To demonstrate the performance of this method, we examine the real part of dynamic α of singlet 1,3-dipole systems having a variety of diradical characters (y). The frequency dispersion of α, in particular in the resonant region, is shown to strongly depend on the exchange-correlation functional as well as on the diradical character. Under sufficiently off-resonant condition, the dynamic α is found to decrease with increasing y and/or the fraction of Hartree−Fock exchange in the exchange-correlation functional, which enhances the spin polarization, due to the decrease in the delocalization effects of π-diradical electrons in the frontier orbital pair. The BS-DFTQME method with the BHandHLYP exchange-correlation functional also turns out to semiquantitatively reproduce the α spectra calculated by a strongly correlated *ab initio* molecular orbital method, i.e., the spin-unrestricted coupled-cluster singles and doubles.

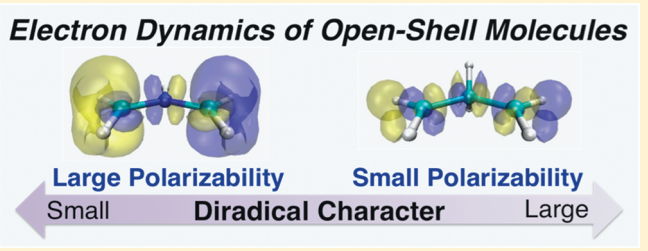

1. INTRODUCTION

Recently, open-shell molecular systems have attracted much attention in a variety of fields of materials science due to their unique electronic structures as well as peculiar chemical-physical functionalities[1] including specific reactivities.[2] These molecules include efficient singlet fission chromophores for dye-sensitized solar cells,[3] the Fe(dipyrazolpyridine)$_2$ system exhibiting light-induced excited spin state trapping,[4] inorganic four-membered heterocyclic compounds,[5] square planar nickel complexes containing two *o*-semiquinonato type ligands,[6] quinoidal oligothiophenes,[7] derivatives of 1,4-bis-(4,5-diphenylimidazol-2-ylidene)-cyclohexa-2,5-diene,[8] and open-shell singlet oligoacenes[9] as well as nanographenes and related structures.[10] Several synthesis strategies also have been developed to design diradicals and multiradicals with tailored spin multiplicity and open-shell character.[11] It was also found that intra- and intermolecular covalent bonds coexist in the solid state due to the open-shell character of the constituent molecules.[12,13] On the basis of the unique electronic structures of open-shell molecular systems, we have recently proposed novel electronic structure - nonlinear optical (NLO) property relationships, i.e., spin multiplicity effects on static second hyperpolarizability (γ),[14a] a significant enhancement of static γ of open-shell singlet systems with intermediate diradical character compared with the closed-shell and complete diradical systems with similar conjugation length,[14b−e] and giant electric field effect on open-shell singlet systems.[14f] There have been lots of theoretical and experimental studies on open-shell molecules with highly active (non)linear optical properties motivated by our structure−property relationships.[15−17] On the other hand, most of the previous theoretical studies on the open-shell NLO have mainly focused on the static (hyper)polarizabilities, except for our recent study on the two-photon absorption peak of a two-site model diradical system.[17] This is due to the difficulty in calculating the reliable excitation energies and transition properties for the ground and excited states of open-shell singlet systems in a well-balanced manner. Therefore, it remains plenty of subjects to be clarified for the dynamic (hyper)polarizability of real open-shell systems.

There already have been several calculation schemes of dynamic (hyper)polarizabilities such as the sum-over-states (SOS),[18] the response theory,[19] the quasi-energy derivative methods,[20] many-mode Floquet theory,[21] numerical Liouville approach,[22] etc. In this study, we present a novel method for calculation and analysis of the (hyper)polarizability of open-shell molecular systems from the viewpoint of the real space electron dynamics. This method rests on a recently proposed exciton description based on the *ab initio* molecular orbital (MO)−configuration interaction singles (CIS) method combined with

Received: January 3, 2011
Revised: February 22, 2011
Published: March 30, 2011

ACS Publications © 2011 American Chemical Society

the quantum master equation method (MOQME),[23a,23b] which can reproduce the time evolution of system population and polarization.[23c−e] This method also has an advantage of including the relaxation effects originating from the weak exciton−phonon coupling in the electron dynamics based on the relaxation theory.[23f,g] The MOQME method is extended so as to treat the open-shell molecular systems based on the broken-symmetry (BS) CIS and the time-dependent density functional theory (TDDFT) within the Tamm-Dancoff approximation (TDA),[24] which are referred to as the BS-MOQME and BS-DFTQME methods, respectively. By using these methods and the nonperturbative definition of (hyper)polarizability,[22] we calculate the real part of dynamic polarizability $\alpha(-\omega;\omega)$ and its density,[25] which represents the spatial linear response of one-electron density. The contribution of each orbital pair, e.g., the highest occupied molecular orbital (HOMO) and the lowest unoccupied molecular orbital (LUMO), to the α and its density is examined in order to clarify the relationship between the diradical character[26] and dynamic α. This is discussed in relation to the diradical character dependence of excitation energy and transition moment obtained analytically by the valence configuration interaction method with a two-site model.[14e,15l,17] As model open-shell systems, several 1,3-dipoles having different diradical characters are examined in order to demonstrate the performance of the present method. We discuss the diradical character and exchange-correlation (xc) functional dependences of frequency dispersion of real part of α in the off-resonant region. We also clarify the reliability of the BS-DFTQME results using the hybrid xc-functionals by comparing these with the strongly correlated *ab initio* MO results. On the basis of these results, we discuss the applicability of the present method to the dynamic response properties of large-size open-shell molecular systems.

2. METHODOLOGY

2.1. Quantum Master Equation (QME) Method and Dynamic Polarizability. We briefly explain the QME method, which can treat the time evolution of system reduced density matrix (RDM) in the adiabatic state basis $\{|\eta\rangle\}$ in the presence of an interaction between the exciton and phonon bath states, e.g., nuclear vibrational modes composed of harmonic oscillators.[27,28] According to the standard method of relaxation theory, we trace over the phonon bath states, which are assumed to be in the thermal equilibrium state at temperature T, and thus derive the QME for the system RDM, $\rho_{\eta\lambda}$, within the Born-Markov approximation[27,28]

$$\frac{d\rho_{\eta\lambda}}{dt} = -i(\omega_\eta - \omega_\lambda)\rho_{\eta\lambda} - \sum_{\sigma\nu}^{M}\Gamma_{\eta\lambda;\sigma\nu}\rho_{\sigma\nu} - F^l\sum_{\sigma}^{M}(\mu^l_{\eta\sigma}\rho_{\sigma\lambda} - \rho_{\eta\sigma}\mu^l_{\sigma\lambda}) \tag{1}$$

and

$$\frac{d\rho_{\eta\eta}}{dt} = -\sum_{\lambda}^{M}\Gamma_{\eta\eta;\lambda\lambda}\rho_{\lambda\lambda} - F^l\sum_{\lambda}^{M}(\mu^l_{\eta\lambda}\rho_{\lambda\eta} - \rho_{\eta\lambda}\mu^l_{\lambda\eta}) \tag{2}$$

Here, M indicates the number of states involving the ground and excited states used in the QME method, ω_η is the eigenfrequency of state $|\eta\rangle$, and $\mu^l_{\eta\lambda}$ indicates the l-th component ($l = x, y, z$) of transition moment between excited states η and λ. $\Gamma_{\eta\lambda;\sigma\nu}$ describes the relaxation from the RDM component $\rho_{\sigma\nu}$ to $\rho_{\eta\lambda}$. We assume that an external plane-wave laser field F polarized in the l-direction is applied to the system in order to generate an electric polarization $P^l(t)$ in the molecular system, which is calculated by $P^l(t) = \mathrm{tr}[\mu^l\rho(t)]$. Then, we can calculate the dynamic polarizability $\alpha_{ll}(-\omega;\omega)$ based on the nonperturbative definition of the polarizability[22]

$$\alpha_{ll}(-\omega;\omega) = \frac{P^l(\omega)}{F^l(\omega)} \tag{3}$$

where $P(\omega)$ and $F(\omega)$ represent the frequency-domain system polarization and incident electric field, respectively, obtained by the Fourier transform of $P(t)$ and $F(t)$. If we employ an appropriate applied field power, the nonperturbative dynamic polarizabilities calculated by the QME method agree precisely with those calculated by the perturbation theory method, e.g., the SOS method.

2.2. BS-MOQME Method. In a similar manner to the formulation of the MOQME method,[23a,b] we present a formulation of the BS-MOQME method. For simplicity, we assume the initial state to be the singlet ground state though the present method can be applied to any high-spin states as the initial state. In the BS-MO formalism, we use different spatial orbitals for different spins. The spin unrestricted (U) Hartree−Fock (HF) singlet determinant in the ground state is represented as

$$\begin{aligned}|^1\Psi_{\mathrm{GS}}\rangle &\equiv |i=1\rangle \equiv |\cdots a\bar{a}b\bar{b}\cdots\rangle \\ &= |\cdots\psi^\alpha_a(\boldsymbol{r})\alpha(\omega)\psi^\beta_a(\boldsymbol{r})\beta(\omega)\psi^\alpha_b(\boldsymbol{r})\alpha(\omega)\psi^\beta_b(\boldsymbol{r})\beta(\omega)\cdots\rangle\end{aligned} \tag{4}$$

where $\psi^\alpha(\boldsymbol{r})$ and $\psi^\beta(\boldsymbol{r})$ are spatial orbitals for α and β spins, respectively, the indices a, b, ... (r, s, ...) indicate the occupied (virtual) orbitals, and the upper bar represents the orbital for β spin. The single excitation configurations from the ground state determinant are classified into the following two types

$$\begin{aligned}|^1\Psi^r_a\rangle &\equiv |i(=a\rightarrow r)\rangle \equiv |\cdots r\bar{a}b\bar{b}\cdots\rangle, \text{ and} \\ |^1\Psi^{\bar{r}}_{\bar{a}}\rangle &\equiv |i'(=\bar{a}\rightarrow\bar{r})\rangle \equiv |\cdots a\bar{r}b\bar{b}\cdots\rangle\end{aligned} \tag{5}$$

The configuration $\{|i\rangle\}$ ($\{|i'\rangle\}$) represents the single excitation from the occupied MO $\psi^\alpha_a(\psi^\beta_a)$ to the virtual MO ψ^α_r (ψ^β_r). The UCIS states $\{|\eta\rangle\}$ can be expanded by these excitation configurations

$$|\eta\rangle = \sum_i C_{i\eta}|i\rangle + \sum_{i'(\neq 1,\, i)} C_{i'\eta}|i'\rangle \tag{6}$$

where $C_{i\eta}$ and $C_{i'\eta}$ are the UCIS expansion coefficients. The UHF singlet determinant, eq 4, does not mix with any single excitation configurations, eq 5. The ground state $|\eta = 1\rangle$ is therefore represented by the UHF singlet determinant $|i = 1\rangle$, where $C_{i=1,\eta=1} = 1$.

The time-evolution of system RDM in the UCIS state basis, $\rho_{\eta\lambda}(t)$, is calculated numerically by solving eqs 1 and 2. Then, the matrix elements, $\rho_{\eta\lambda}(t)$, are converted into those, $\rho_{ij}(t)$, in the one-exciton configuration basis $\{|i\rangle\}$ by using eq 6. The one-electron reduced density $\rho(\boldsymbol{r},t)$ at the initial state ($t = 0$) is represented by that for the ground state determinant [$|\eta = 1\rangle = |i = 1\rangle$], i.e., $\rho(\boldsymbol{r},0) = \Sigma_a|\psi^\alpha_a(\boldsymbol{r})|^2 + \Sigma_a|\psi^\beta_a(\boldsymbol{r})|^2 = d_{11}(\boldsymbol{r})$, where $d_{ij}(\boldsymbol{r})$ is the reduced one-electron density matrix in the configuration basis $\{|i\rangle\}$. The polarization density, which is defined as the difference between the one-electron density at time t and that at the initial time,[23b] is

therefore calculated by

$$\rho_{\mathrm{pol}}(\boldsymbol{r},t) \equiv \rho(\boldsymbol{r},t) - d_{11}(\boldsymbol{r}) = \sum_{i(\neq 1)} [d_{ii}(\boldsymbol{r}) - d_{11}(\boldsymbol{r})]\rho_{ii}(t) + 2\sum_{i(\neq 1)} d_{1i}(\boldsymbol{r})\rho_{1i}^{\mathrm{real}}(t) + 2\sum_{i<j(i,j\neq 1)} d_{ij}(\boldsymbol{r})\rho_{ij}^{\mathrm{real}}(t) + \sum_{i'(\neq 1,i)} [d_{i'i'}(\boldsymbol{r}) - d_{11}(\boldsymbol{r})]\rho_{i'i'}(t) + 2\sum_{i'(\neq 1,i)} d_{1i'}(\boldsymbol{r})\rho_{1i'}^{\mathrm{real}}(t) + 2\sum_{i'<j'(i',j'\neq 1,i,j)} d_{i'j'}(\boldsymbol{r})\rho_{i'j'}^{\mathrm{real}}(t) \equiv \rho_{\mathrm{pol}}^{\alpha}(\boldsymbol{r},t) + \rho_{\mathrm{pol}}^{\beta}(\boldsymbol{r},t) \tag{7}$$

Here, the superscript "real" means the real part of the density matrix, and we use the relation, $\rho_{11}(t) = 1 - \Sigma_{i(\neq 1)}\rho_{ii}(t) - \Sigma_{i'(\neq 1,i)}\rho_{i'i'}(t)$, for the one-exciton population generated by photoabsorption. Because $\{|i\rangle\}$ and $\{|i'\rangle\}$ indicate $\alpha\rightarrow\alpha$ and $\beta\rightarrow\beta$ excitation configurations, respectively, we can partition the total polarization density into the α- and β-electron contributions, $\rho_{\mathrm{pol}}^{\alpha}(\boldsymbol{r},t)$ and $\rho_{\mathrm{pol}}^{\beta}(\boldsymbol{r},t)$. For example, the one-electron density matrix $d_{ij}(\boldsymbol{r})$ involved in the $\rho_{\mathrm{pol}}^{\alpha}(\boldsymbol{r},t)$ can be defined by using the occupied $\{\psi_a^{\alpha}(\boldsymbol{r}), \psi_b^{\alpha}(\boldsymbol{r}),\cdots\}$ and virtual $\{\psi_r^{\alpha}(\boldsymbol{r}), \psi_s^{\alpha}(\boldsymbol{r}),\cdots\}$ MOs. The polarization density for α electrons is given by

$$\rho_{\mathrm{pol}}^{\alpha}(\boldsymbol{r},t) = \sum_{i(a\rightarrow r)(\neq 1)} \left[\left(|\psi_r^{\alpha}(\boldsymbol{r})|^2 - |\psi_a^{\alpha}(\boldsymbol{r})|^2 \right)\rho_{ii}(t) + 2\psi_a^{\alpha}(\boldsymbol{r})\psi_r^{\alpha}(\boldsymbol{r})\rho_{1i}^{\mathrm{real}}(t) + 2\sum_{j(a\rightarrow s)(>i)} \psi_r^{\alpha}(\boldsymbol{r})\psi_s^{\alpha}(\boldsymbol{r})\rho_{ij}^{\mathrm{real}}(t) - 2\sum_{j(b\rightarrow r)(>i)} \psi_a^{\alpha}(\boldsymbol{r})\psi_b^{\alpha}(\boldsymbol{r})\rho_{ij}^{\mathrm{real}}(t) \right] \tag{8}$$

The similar formula is obtained for β electrons.

We can appropriately define the relationship between the electron $[\rho_{\mathrm{elec}}^{\sigma}(\boldsymbol{r},t)]$ and hole $[\rho_{\mathrm{hole}}^{\sigma}(\boldsymbol{r},t)]$ densities as $\rho_{\mathrm{pol}}^{\sigma}(\boldsymbol{r},t) \equiv \rho_{\mathrm{elec}}^{\sigma}(\boldsymbol{r},t) - \rho_{\mathrm{hole}}^{\sigma}(\boldsymbol{r},t)$ $(\sigma = \alpha,\beta)$,[23b] which implies that the spatial separation of the electron and hole density distributions gives the polarization density. Using eq 8 and this relationship, we define $\rho_{\mathrm{elec}}^{\alpha}(\boldsymbol{r},t)$ and $\rho_{\mathrm{hole}}^{\alpha}(\boldsymbol{r},t)$ as[23b]

$$\rho_{\mathrm{elec}}^{\alpha}(\boldsymbol{r},t) = \sum_{i(a\rightarrow r)(\neq 1)} \left[|\psi_r^{\alpha}(\boldsymbol{r})|^2\rho_{ii}(t) + \psi_a^{\alpha}(\boldsymbol{r})\psi_r^{\alpha}(\boldsymbol{r})\rho_{1i}^{\mathrm{real}}(t) + 2\sum_{j(a\rightarrow s)(>i)} \psi_r^{\alpha}(\boldsymbol{r})\psi_s^{\alpha}(\boldsymbol{r})\rho_{ij}^{\mathrm{real}}(t) \right] \tag{9}$$

and

$$\rho_{\mathrm{hole}}^{\alpha}(\boldsymbol{r},t) = \sum_{i(a\rightarrow r)(\neq 1)} \left[|\psi_a^{\alpha}(\boldsymbol{r})|^2\rho_{ii}(t) - \psi_a^{\alpha}(\boldsymbol{r})\psi_r^{\alpha}(\boldsymbol{r})\rho_{1i}^{\mathrm{real}}(t) + 2\sum_{j(b\rightarrow r)(>i)} \psi_a^{\alpha}(\boldsymbol{r})\psi_b^{\alpha}(\boldsymbol{r})\rho_{ij}^{\mathrm{real}}(t) \right] \tag{10}$$

The similar definitions are presented for β electron and hole densities. We summarize the relations among electron, hole, and polarization densities as follows

$$\rho_{\mathrm{X}}(\boldsymbol{r},t) \equiv \rho_{\mathrm{X}}^{\alpha}(\boldsymbol{r},t) + \rho_{\mathrm{X}}^{\beta}(\boldsymbol{r},t) \ (\mathrm{X} = \mathrm{elec}, \mathrm{hole}, \mathrm{pol}) \tag{11}$$

and

$$\rho_{\mathrm{pol}}^{\sigma}(\boldsymbol{r},t) \equiv \rho_{\mathrm{elec}}^{\sigma}(\boldsymbol{r},t) - \rho_{\mathrm{hole}}^{\sigma}(\boldsymbol{r},t) \ (\sigma = \alpha,\beta) \tag{12}$$

Because the spin density is defined by the difference between α and β one-electron densities (see eqs 7 and 13), we can obtain a dynamic spin density, $\rho^{\mathrm{spin}}(\boldsymbol{r},t)$, using the α and β polarization densities $[\rho_{\mathrm{pol}}^{\sigma}(\boldsymbol{r},t), (\sigma = \alpha,\beta)]$ and the α/β reduced one-electron density matrices $[d_{11}^{\sigma}(\boldsymbol{r}),(\sigma = \alpha,\beta)]$

$$\begin{aligned}\rho^{\mathrm{spin}}(\boldsymbol{r},t) &\equiv \rho^{\alpha}(\boldsymbol{r},t) - \rho^{\beta}(\boldsymbol{r},t)\\ &= d_{11}^{\alpha}(\boldsymbol{r}) - d_{11}^{\beta}(\boldsymbol{r}) + \rho_{\mathrm{pol}}^{\alpha}(\boldsymbol{r},t) - \rho_{\mathrm{pol}}^{\beta}(\boldsymbol{r},t)\\ &= \sum_a (|\psi_a^{\alpha}(\boldsymbol{r})|^2 - |\psi_a^{\beta}(\boldsymbol{r})|^2) + \rho_{\mathrm{pol}}^{\alpha}(\boldsymbol{r},t) - \rho_{\mathrm{pol}}^{\beta}(\boldsymbol{r},t)\\ &= \rho^{\mathrm{spin}}(\boldsymbol{r},0) + \rho_{\mathrm{pol}}^{\mathrm{spin}}(\boldsymbol{r},t)\end{aligned} \tag{13}$$

where $\rho_{\mathrm{pol}}^{\mathrm{spin}}(\boldsymbol{r},t)$ indicates the spin polarization density, which represents the deviation of spin density at time t from the initial spin density distribution. In the previous study,[23e] we have employed the present method based on the BS-MOQME in order to analyze electron-, hole-, and spin-density dynamics of the simplest open-shell molecular model, i.e., H_2 dissociation model. At a large interatomic distance of H_2 under irradiation of resonant electric field, we have observed the decrease of spin density on each H atom because the diradical (covalent) component of the (time-dependent) wave function decreases due to the field-induced superposition of the diradical ground and the ionic excited states.[23e] Such population dynamics are found to be induced by the resonant electric field. Alternatively, we here focus on the off-resonant electron dynamics, which are characterized by the real part of off-resonant dynamic polarizability.

2.3. QME Dynamics Based on the BS-TDDFT within the TDA Calculations. The TDDFT within the TDA is here summarized from the viewpoint of the connection to the QME method. Within the TDA, the de-excitation terms appearing in the standard TDDFT formalism are neglected.[24c] The TDA working equation takes the following eigenvalue equation form[24c]

$$\boldsymbol{AX} = \omega\boldsymbol{X} \tag{14}$$

where the matrix $\boldsymbol{A}$ is defined as follows

$$\boldsymbol{A}_{ra\sigma,sb\tau} = \delta_{ab}\delta_{rs}\delta_{\sigma\tau}(\varepsilon_{r\sigma} - \varepsilon_{a\tau}) + (\psi_r^{\sigma}\psi_a^{\sigma}|\psi_b^{\tau}\psi_s^{\tau}) + \left(\psi_r^{\sigma}\psi_a^{\sigma}\left|\frac{\delta^2 E_{\mathrm{XC}}}{\delta\rho_{\sigma}\delta\rho_{\tau}}\right|\psi_b^{\tau}\psi_s^{\tau}\right) \tag{15}$$

Here, E_{XC}, ψ_{pq}^{σ}, ε_{pq}, and ρ_p represent the exchange-correlation energy, Kohn−Sham orbital, orbital energy, and one-electron density, respectively, and symbols σ and τ depict spin (α and/or β). By diagonalizing the matrix $\boldsymbol{A}$, we obtain the excitation energies as eigenvalues and the excitation amplitudes as eigenstate vectors. This equation is practically the same form as the CIS working equation. Indeed, when we take the HF (exact) exchange energy functional as E_{XC}, we obtain the same results as those by the CIS method. We thus regard the excitation amplitudes as the CI coefficients. As a result, we can employ the spin-unrestricted Kohn−Sham orbitals, excitation amplitudes, excitation energies, and transition moments in the BS-MOQME

working equations (eqs 1 − 3) and various densities for analysis (eqs 7 − 13). Note that although the transition moments between the excited states are generally unavailable within the linear response TDDFT, we can reasonably neglect these contributions to the off-resonant linear polarizability focused in this study.

2.4. Dynamic Polarizability Density Analysis. Similar to the system polarization $P(t)$, the polarization density, $\rho_{pol}(\boldsymbol{r},t)$, is also expanded by the Fourier components. The frequency-domain polarization density $\rho_{pol}(\boldsymbol{r},\omega)$ is defined by the Fourier transform of $\rho_{pol}(\boldsymbol{r},t)$. Therefore, the dynamic polarizability density, $\rho^{(1)}(\boldsymbol{r},-\omega;\omega)$, which represents linear response part of one-electron density to the applied field $F \equiv (F^l)$, is expressed by[25]

$$\rho^{(1)}(\boldsymbol{r}, -\omega;\omega) = \frac{\rho_{pol}(\boldsymbol{r},\omega)}{F(\omega)} \tag{16}$$

the spatial integration of which gives the system polarizability $\alpha(-\omega;\omega)$ $[\equiv, \alpha_{ll}(-\omega;\omega)]$

$$\alpha(-\omega;\omega) = -\int r\rho^{(1)}(\boldsymbol{r}, -\omega;\omega)d\boldsymbol{r} \tag{17}$$

where $r \equiv r^l$, and the real(imaginary) part of $\rho^{(1)}(\boldsymbol{r},-\omega;\omega)$ leads to real(imaginary) $\alpha(-\omega;\omega)$. In this study, we consider the real parts of $\rho^{(1)}(\boldsymbol{r},-\omega;\omega)$ and $\alpha(-\omega;\omega)$, which indicate real parts hereafter, because we focus on the off-resonant $\alpha(-\omega;\omega)$. The plot of $\rho^{(1)}(\boldsymbol{r},-\omega;\omega)$ is useful to investigate the structure−property relationship in the linear optical property of molecules because the spatial distribution of $\rho^{(1)}(\boldsymbol{r},-\omega;\omega)$ represents the field-induced increase and decrease regions of electron density. For a pair of localized α densities $[\rho^{(1)}(\boldsymbol{r},-\omega;\omega)]$ with positive and negative values, the sign of the contribution to α is positive when the direction from positive to negative α density coincides with the positive direction of the coordinate system. The sign becomes negative in the opposite case. The amplitudes of the contribution associated with this pair of α densities is proportional to the distance between them. Practically, $\rho^{(1)}(\boldsymbol{r},-\omega;\omega)$ is calculated by the following procedure. We first compute the linear response parts of the RDM elements, $\rho_{ij}^{(1)}(-\omega;\omega) = \rho_{ij}(\omega)/F(\omega)$, from the frequency-domain RDM in the one-exciton basis, $\{\rho_{ij}(\omega)\}$. Substituting them into the first-order densities in eq 7, we obtain the dynamic α density

$$\begin{aligned}\rho^{(1)}(\boldsymbol{r}, -\omega;\omega) \equiv& \sum_{i(\neq 1)}[d_{ii}(\boldsymbol{r}) - d_{11}(\boldsymbol{r})]\rho_{ii}^{(1)}(-\omega;\omega) \\ &+ 2\sum_{i=2} d_{1i}(\boldsymbol{r})\rho_{1i}^{(1)}(-\omega;\omega) \\ &+ 2\sum_{i<j(i,j\neq 1)} d_{ij}(\boldsymbol{r})\rho_{ij}^{(1)}(-\omega;\omega) + \sum_{i'(\neq 1,i)}[d_{i'i'}(\boldsymbol{r}) \\ &- d_{11}(\boldsymbol{r})]\rho_{i'i'}^{(1)}(-\omega;\omega) + 2\sum_{i'(\neq 1,i)} d_{1i'}(\boldsymbol{r})\rho_{1i'}^{(1)}(-\omega;\omega) \\ &+ 2\sum_{i'<j'(i',j'\neq 1,i,j)} d_{i'j'}(\boldsymbol{r})\rho_{i'j'}^{(1)}(-\omega;\omega)\end{aligned} \tag{18}$$

On the other hand, the frequency-dependent system polarization is represented by $P(\omega) = \mathrm{tr}[\mu\rho(\omega)]$, where $P(\omega)$ and μ are the l-th components of polarization and transition moment operator, respectively. The dynamic α is therefore calculated

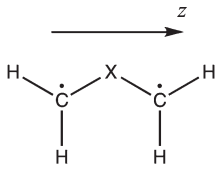

X = NH (**1**), O (**2**), CO (**3**), CH_2 (**4**)

Figure 1. Schematic structures of 1,3-dipole systems involving central X = NH (**1**), O (**2**), C═O (**3**), and CH_2 (**4**).

by using the linear response part of RDM $\{\rho_{ij}^{(1)}(-\omega;\omega)\}$ as

$$\begin{aligned}\alpha(-\omega;\omega) =& \mathrm{tr}[\mu\rho^{(1)}(-\omega;\omega)] = 2\sum_{j(\neq 1)}\mu_{1j}\rho_{j1}^{(1)}(-\omega;\omega) \\ &+ 2\sum_{j'(\neq 1,j)}\mu_{1j'}\rho_{j'1}^{(1)}(-\omega;\omega) + \sum_{i(\neq 1),j(\neq 1)}\mu_{ij}\rho_{ji}^{(1)}(-\omega;\omega) \\ &+ \sum_{i'(\neq 1,i),j'(\neq 1,j)}\mu_{i'j'}\rho_{j'i'}^{(1)}(-\omega;\omega)\end{aligned} \tag{19}$$

where $\mu_{ij} = -\int r d_{ij}(\boldsymbol{r})d\boldsymbol{r}$. Neglecting the transition moments between the excited states, which is a reasonable approximation in the case of off-resonant ground state $\alpha(-\omega;\omega)$, eq 19 is expressed by

$$\begin{aligned}\alpha(-\omega;\omega) &\approx 2\sum_i \mu_{1i}\rho_{i1}^{(1)}(-\omega;\omega) + 2\sum_{i'(\neq i)}\mu_{1i'}\rho_{i'1}^{(1)}(-\omega;\omega) \\ &= \sum_{ar}\alpha^{a\rightarrow r}(-\omega;\omega) + \sum_{\bar{a}\bar{r}}\alpha^{\bar{a}\rightarrow\bar{r}}(-\omega;\omega)\end{aligned} \tag{20}$$

where the basis $|i\rangle$ $(|i'\rangle)$ is connected to the excitation from occupied $a(\bar{a})$ to virtual $r(\bar{r})$ orbital. Using eq 20, we can analyze the contribution from each orbital pair to the dynamic polarizability. In α spin case, from eq 17 and the relation $\mu_{1i} = -\int r d_{1i}(\boldsymbol{r})d\boldsymbol{r} = -\int r\psi_a^{\alpha}(\boldsymbol{r})\psi_r^{\alpha}(\boldsymbol{r})d\boldsymbol{r}$ $(i{=}a\rightarrow r)$, we have

$$\begin{aligned}\alpha^{a\rightarrow r}(-\omega;\omega) &= -\int r\rho_{a\rightarrow r}^{(1)}(\boldsymbol{r}, -\omega;\omega)d\boldsymbol{r} \\ &= -2\int r d_{1i}(\boldsymbol{r})\rho_a^{(1)}(-\omega;\omega)d\boldsymbol{r}\end{aligned} \tag{21}$$

It is noted that this relation is also derived using eq 8 when excited state population $\rho_{ii}(t)$ $(i > 1)$ and transition density $\rho_{ij}(t)$ $(i,j > 1)$ are negligible, i.e., in the off-resonant case. The $\rho_{a\rightarrow r}^{(1)}(\boldsymbol{r},-\omega;\omega)$ represents the contribution of an orbital pair (a, r) to the polarizability density. By analyzing $\alpha^{a\rightarrow r}(-\omega;\omega)$ and its spatial distribution $\rho_{a\rightarrow r}^{(1)}(\boldsymbol{r},-\omega;\omega)$, we can extract the orbital pair(s) primarily contributing to the dynamic polarizability. This procedure of analysis is applied to the case of β spin in the same manner.

3. CALCULATIONS

3.1. Calculated Model Systems. In order to demonstrate the performance of the BS-DFTQME method, we investigate the frequency dispersion of polarizabilities, $\alpha(-\omega;\omega)$ $[\equiv \alpha_{zz}(-\omega;\omega)]$, along the spin polarization axis (z) of simple π-conjugated diradical systems, i.e, 1,3-dipoles (see Figure 1). Their geometries are optimized at the UB3LYP/6-31G** level of

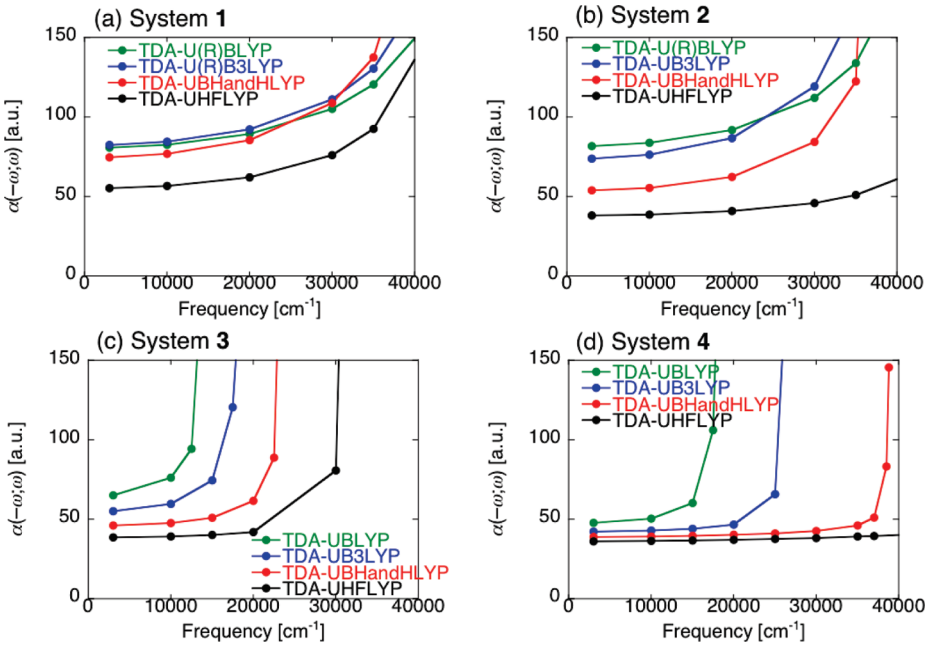

Figure 2. Frequency dispersion of real part of $\alpha(-\omega;\omega)$ [a.u.] of systems **1** (a), **2** (b), **3** (c), and **4** (d) calculated by the BS-DFTQME method using the TDA-UX (X = BLYP, B3LYP, BHandHLYP, and HFLYP) results.

approximation under the constraint of C_{2v} symmetry.[16g,29] It is well-known that if the central moiety X involves a heteroatom like NH (**1**), O (**2**), and C═O (**3**), the contribution of ionic resonance form is important and spin delocalization effects are induced, leading to the singlet ground states with small diradical character, whereas in the case of X = CH_2 (**4**), the ground state becomes the triplet state due to the large spin polarization effect. Such possible diradical and zwitterionic resonance forms indicate that these molecules exhibit a wide range of diradical characters by changing X. The diradical character y related to the HOMO and LUMO in the singlet state is defined by twice the weight of the doubly excited configuration in the multiconfigurational (MC)-SCF theory[26a] and is formally expressed in the case of the spin-projected UHF (PUHF) theory as[26b,c]

$$y = 1 - \frac{2T}{1+T^2}, \text{ where } T = \frac{n_{\mathrm{HOMO}} - n_{\mathrm{LUMO}}}{2} \qquad (22)$$

Here, T is the orbital overlap between the corresponding orbital pairs and can be calculated using the occupation numbers (n) of UHF natural orbitals (UNOs). The diradical character takes values between 0 and 1, which correspond to the closed-shell and pure diradical states in the singlet state, respectively. The diradical characters for these 1,3-dipole models calculated from the UNOs/6-31G** are indeed shown to cover a wide range: y = 0.15 [X = NH (**1**)], 0.35 [X = O (**2**)], 0.59 [X = CO (**3**)], and 0.91 [X = CH_2 (**4**)].[16g]

3.2. Frequency Dispersion of Polarizability. The excitation energies and transition moments of systems **1**−**4** are calculated by the spin-unrestricted TD(U)DFT/TDA method within the frozen core approximation using the 6-31G** basis set. The BLYP, B3LYP, and BHandHLYP as well as the HFLYP xc-functionals are employed in order to clarify the xc-functional dependence of polarizability α. Hereafter, we refer to them as TDA-UY (Y = BLYP, B3LYP, BHandHLYP, and HFLYP). All the TDA-UY calculations are performed by the NWChem 5.1.1 program package.[30] We obtain the lowest-lying 500 excited states to be considered in the QME working equations (eqs 1 and 2). The UHFLYP and UBHandHLYP methods provide the BS solutions for all the systems, while the UB3LYP (UBLYP) method does not give the BS solution for system **1** (systems **1** and **2**), the feature of which is indicated by the notations U(R)BLYP or U(R)B3LYP. This is due to the variation in the triplet instability point depending on the xc-functionals.[14b,16g,16h]

The relaxation factors, Γ, appearing in eqs 1 and 2 are set to zero, while we set an additional damping parameter, a full width at half-maximum for each excited state, as 0.02 eV, which does not affect the relative comparison of the results. Equations 1 and 2 are then numerically solved by the sixth-order Runge−Kutta method in the presence of a continuous wave laser field, polarized in the z-direction, with a power of 1 MW/cm^2. In order to reduce the numerical error to within 1% of the dynamic α calculated by the SOS method, the time-evolution of RDM is calculated up to 10−200 optical cycles, each cycle of which is divided into 200−500 time steps in the Runge−Kutta method. We thus predict that the time series of $P(t)$ and $\rho(t)$ can provide sufficiently converged amplitudes of $P(t)$ in the numerical Fourier transform.[22]

Figure 2 shows the frequency dispersion of the real α values (z-component) of **1**-**4** by the TDA-UY method up to ω = 40000 cm^{-1}. They are shown to strongly depend on the xc-functional as well as on the diradical character. For system **1** with the smallest diradical character (y = 0.15), the TDA-U(R)BLYP and TDA-U(R)B3LYP results are shown to be very close to each other at the off-resonant frequency (81 and 82 a.u., respectively, at ω = 3000 cm^{-1}). It is found at ω = 3000 cm^{-1} that the TDA-UBHandHLYP result (75 a.u.) is slightly smaller than them, while the TDA-UHFLYP result (51 a.u.) is significantly reduced, i.e., about 63% of the TDA-U(R)BLYP value. The frequency dispersion of α values becomes significant around ω = 30000 cm^{-1} for all results, particularly for the UBHandHLYP result. Indeed, in contrast to the case of ω = 3000 cm^{-1}, at ω = 35000 cm^{-1}, the order of α amplitude becomes as TDA-UBHandHLYP (137 a.u.) > TDA-U(R)B3LYP (130 a.u.) > TDA-U(R)BLYP (120 a.u.) > TDA-UHFLYP

dx.doi.org/10.1021/jp200056m |J. Phys. Chem. A 2011, 115, 3565–3575

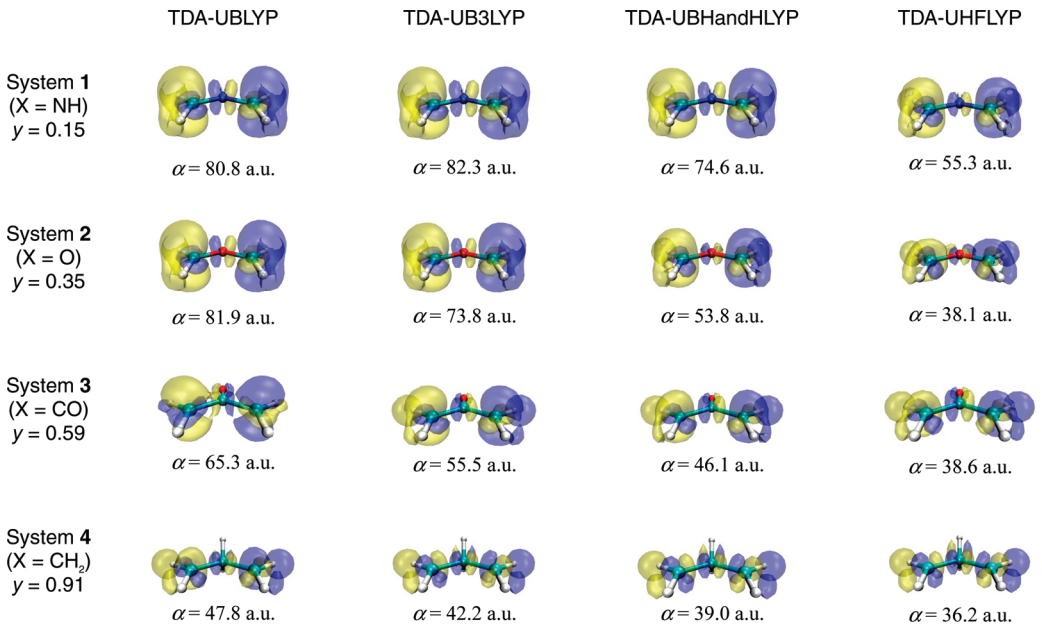

Figure 3. Spatial distributions of dynamic polarizability density (calculated at $\omega = 3000\ \mathrm{cm}^{-1}$), $\rho^{(1)}(\boldsymbol{r},-\omega;\omega)$ (eq 18), of 1,3-dipole systems calculated by the TDA-UX (X = BLYP, B3LYP, BHandHLYP, and HFLYP) methods. Yellow (blue) surface shows the +0.1 a.u. (−0.1 a.u.) isosurface of $\rho^{(1)}(\boldsymbol{r},-\omega;\omega)$.

(80 a.u.). This change in the dispersion behavior indicates that the resonant frequencies and peak intensities significantly depend on the xc-functionals.

It is found that although the relative amplitudes of α among these methods for system **2** ($y = 0.39$) are different from those for system **1**, the frequency dispersion behaviors of α for system **2** are similar to those for system **1**, except for the TDA-UHFLYP results. Indeed, under the sufficiently off-resonant condition ($\omega = 3000\ \mathrm{cm}^{-1}$), the calculated α values are shown to be in the order of TDA-U(R)BLYP (82 a.u.) > TDA-UB3LYP (74 a.u.) > TDA-UBHandHLYP (54 a.u.) > TDA-UHFLYP (36 a.u.), while all the α values except for the TDA-UHFLYP result show significant increase behaviors around $\omega = 30000\ \mathrm{cm}^{-1}$. The TDA-UBHandHLYP α is shown to increase more rapidly than other methods as increasing the frequency, and then the order becomes TDA-UB3LYP (171 a.u.) > TDA-U(R)BLYP (134 a.u.) > TDA-UBHandHLYP (122 a.u.) > TDA-UHFLYP (44 a.u.) at $\omega = 35000\ \mathrm{cm}^{-1}$. In contrast, the frequency dispersion of the TDA-UHFLYP α value is shown to be negligible as compared to the others from 3000 to 35000 cm^{-1}. This indicates that the TDA-UHFLYP method provides a much higher resonant frequency than the other methods.

The results of systems **3** ($y = 0.59$) and **4** ($y = 0.91$) having large diradical characters show more significant xc-functional dependences for the frequency dispersions than those for systems **1** and **2**, though the off-resonant α values become much closer to each other among these methods. For example, it turns out for system **3** that the minimum α value (39 a.u.) calculated by the TDA-UHFLYP method achieves more than 59% of the maximum α (65 a.u.) by the TDA-UBLYP method, whereas the resonant frequencies of different functionals are distributed around the region of 15000−31000 cm^{-1} as seen from Figure 2. Such tendency becomes more emphasized for system **4**. At $\omega = 3000\ \mathrm{cm}^{-1}$, the minimum α value (36 a.u.) calculated by the TDA-UHFLYP method achieves more than 75% of the maximum α (48 a.u.) by the TDA-UBLYP method, whereas the TDA-UHFLYP resonant frequency is predicted to be higher than 40000 cm^{-1}, which is far from the TDA-UBLYP one (18000 cm^{-1}). We therefore discuss the reliability of resonant frequencies calculated by the present methods in the Section 3.4 in comparison with the strongly correlated results.

3.3. Polarizability Density Analysis. Figure 3 shows the isosurfaces of the dynamic polarizability density (eq 18) calculated at the TDA-UY levels of approximation at $\omega = 3000\ \mathrm{cm}^{-1}$. The yellow and blue isosurfaces represent the positive and negative α density distributions, respectively. Similar to the previous results, it is found for all the systems that the sign of π-electron contribution (positive) is opposite to that of σ-electron contribution.[14a,c,16a,16b] We first address the xc-functional dependence of the α density. Because the HF exchange in the spin-unrestricted scheme is known to emphasize the spin-polarization effect, the unpaired π-electrons tend to be localized in the both-end region of the system as increasing the fraction of HF exchange. Considering the diradical character dependence of α of model singlet diradical systems,[16i] such exaggerated spin-polarization is predicted to cause the decrease of the both-end unpaired π-electron contributions to α. Indeed, the TDA-UHFLYP method is shown to undershoot the contributions of π-electrons in the both-end region of systems **1** and **2** with relatively small diradical characters, as compared to the TDA-UBLYP, -UB3LYP, and -UBHandHLYP results. On the other hand, all the methods except for TDA-UHFLYP method are shown to provide, at least, qualitatively the same diradical character dependence of density distributions for these systems.

We next investigate the diradical character dependence of α density distribution obtained by the TDA-UBLYP, -UB3LYP, and -UBHandHLYP methods. Systems **1** and **2** exhibit large positive and negative α densities originating from the both-end π-electron regions, which represent the virtual charge transfer between the both-end π-radical electrons. Such both-end positive and negative π-electron α densities are shown to decrease with the increase of diradical character. Indeed, for systems **3** and

dx.doi.org/10.1021/jp200056m |J. Phys. Chem. A 2011, 115, 3565–3575

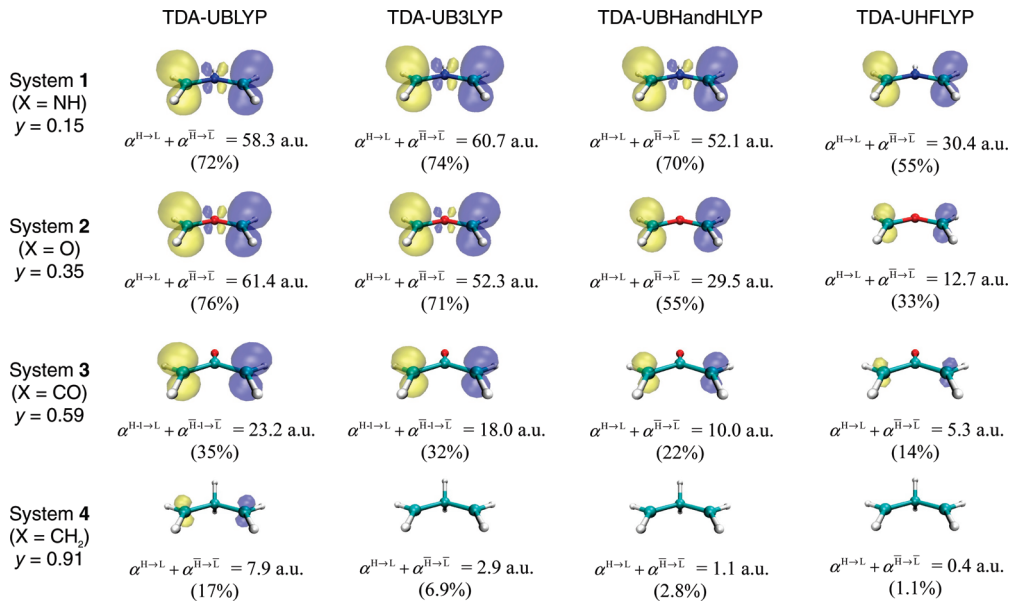

Figure 4. Spatial distributions of dynamic polarizability density (calculated at ω = 3000 cm^{-1}) contributed from HOMO (H) and LUMO (L), $\rho^{(1)}_{H\to L}(r,-\omega;\omega) + \rho^{(1)}_{\bar{H}\to\bar{L}}(r,-\omega;\omega)$, and corresponding $\alpha^{H\to L} + \alpha^{\bar{H}\to\bar{L}}$ (eq 21), where the upper-bar represents the β-spin. Yellow (blue) surface shows the +0.1 a.u. (−0.1 a.u.) isosurface of $\rho^{(1)}_{H\to L}(r,-\omega;\omega)$. Values in round parentheses represent the ratios of the polarizabilities contributed from the H-L pair, i.e., $(\alpha^{H\to L}+\alpha^{\bar{H}\to\bar{L}})/\alpha$(total). For system **3**, we plot the primary contributing pair, H-1 and L, in the TDA-UBLYP and TDA-UB3LYP calculations.

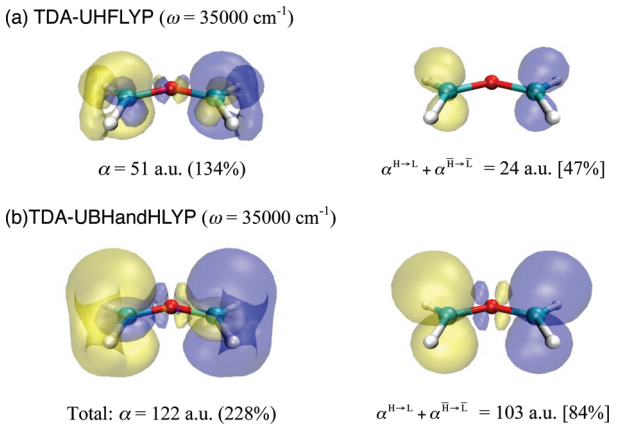

Figure 5. Dynamic polarizability density maps (at ω = 35000 cm^{-1}) of system **2** at the TDA-UHFLYP, (a), and TDA-UBHandHLYP, (b), levels of approximation. Left- and right-hand sides of the figure represent the total and H-L pair polarizability densities, respectively. Yellow (blue) surface shows the +0.1 (−0.1) a.u. isosurface of $\rho^{(1)}_{H\to L}(r,-\omega;\omega)$. Values in round [square] parentheses represent the increase ratios $\alpha(\omega$ = 35000 cm$^{-1})/\alpha(\omega$ = 3000 cm$^{-1})$ [the ratios of the polarizabilities contributed from the H-L pair, i.e., $(\alpha^{H\to L}+\alpha^{\bar{H}\to\bar{L}})/\alpha$(total)].

4, the both-end π-electron density amplitudes are shown to be significantly reduced, and, in particular for system **4**, an alternation in sign of α densities is observed along the C-X-C bonds, which significantly suppresses the virtual charge transfer between the both-end regions. These results indicate that the α values of these systems are primarily described by the contributions of both-end α densities, the amplitudes of which are determined by the degree of localization, i.e., diradical character, of π-radical electrons in the both-end region. Such feature is similar to the diradical character dependence of one-photon absorption peaks obtained by the valence configuration interaction method with a two-site model,[14e,15l,17] though the one-photon peak is described by the imaginary part of α.

In order to clarify the origin of such diradical character dependence of α and its density, we investigate the contributions of the frontier orbital, e.g., HOMO−LUMO, pair to them. For these systems, the delocalized π-electrons (having the intermediate diradical character) are expected to be more easily fluctuated by the external field than the bonding σ-electrons. In the present case, such frontier orbital pair is found to be composed of π-bonding and antibonding orbitals. Figure 4 shows the α density maps (at ω = 3000 cm^{-1}) of HOMO (H)-LUMO (L) contributions, $\rho^{(1)}_{H\to L}(r,-\omega;\omega) + \rho^{(1)}_{\bar{H}\to\bar{L}}(r,-\omega;\omega)$, and their corresponding α values $\alpha^{H\to L} + \alpha^{\bar{H}\to\bar{L}}$ defined by eq 21. It is found for system **3** that the primary contributing pair is not H → L but H−1 → L (then, contributing to y) at the TDA-UBLYP and -UB3LYP levels of approximation, so that the results of H−1 → L pair are shown in these cases. Apparently, the α density amplitudes of these frontier orbtal pairs decrease with the increase of the diradical character. Judging from these density maps and the contribution ratios of the frontier orbitals, i.e., $(\alpha^{H\to L}+\alpha^{\bar{H}\to\bar{L}})/\alpha$(total) (shown in the parentheses), the large positive and negative α densities in the both-end regions of systems **1** and **2** shown in Figure 3 originate in the contribution of H-L pair. On the other hand, for systems **3** and **4** with large diradical characters, the unpaired π-electrons tend to be localized on the both-end C atoms since the fraction of covalent (diradical) electronic structure increases. This causes the relative reduction of the contribution of the frontier orbital pair in such systems.

We next show an example of the α density analysis for the xc-functional dependence of the frequency dispersion of α using the results of system **2**. We compare the α densities of system **2** calculated by the TDA-UHFLYP and TDA-UBHandHLYP methods at ω = 35000 cm^{-1} (see Figure 5). The α values at ω = 35000 cm^{-1} amount to 134% (TDA-UHFLYP) and 228%

dx.doi.org/10.1021/jp200056m |J. Phys. Chem. A 2011, 115, 3565–3575

(TDA-UBHandHLYP) of those at $\omega = 3000\ \mathrm{cm}^{-1}$, respectively. Compared to the α densities at $\omega = 3000\ \mathrm{cm}^{-1}$ (see Figure 3), the amplitudes of both-end positive and negative α densities at $\omega = 35000\ \mathrm{cm}^{-1}$ are shown to be significantly enhanced for the TDA-UBHandHLYP result, while such significant increase is not observed for the TDA-UHFLYP result. The enhancement of α at $\omega = 35000\ \mathrm{cm}^{-1}$ calculated by the TDA-UBHandHLYP method is primarily attributed to the increase of the H-L pair contribution: the ratio of H-L pair contribution increases from 55% ($\omega = 3000\ \mathrm{cm}^{-1}$) to 84% ($\omega = 35000\ \mathrm{cm}^{-1}$). In contrast, for the TDA-UHFLYP result, we cannot observe such significant enhancement of H-L pair contribution: 33% ($\omega = 3000\ \mathrm{cm}^{-1}$) to 47% ($\omega = 35000\ \mathrm{cm}^{-1}$). This is because $\omega = 35000\ \mathrm{cm}^{-1}$ remains to be in a sufficiently off-resonant region in the TDA-UHFLYP result (see also Figure 2b).

3.4. Applicability of BS-DFTQME Method. Finally, we discuss the applicability of the BS-DFTQME method to the calculation of α of open-shell singlet systems. We here focus on the reliability of TDA-UDFT calculations since the numerical stability of the nonperturbative definition of (hyper)polarizabilities has been well discussed in the previous studies.[22]

At first, we compare the results in the off-resonant region ($\omega = 3000\ \mathrm{cm}^{-1}$) with the static α calculated by the finite-field method using the strongly correlated *ab initio* MO methods, i.e., the spin-unrestricted coupled cluster singles and doubles (UCCSD) and that with perturbative triples [UCCSD(T)] methods. Such comparison is meaningful since the real part of dynamic α in the sufficiently off-resonant region approximately coincides with that in the static limit. Table 1 lists the static α values of systems **1**−**4** calculated at the UCCSD and UCCSD(T) level of approximations. The UCCSD and UCCSD(T) results are shown to be in good agreement with each other except for the slight deviation in system **2**. Both methods predict the decrease behavior of α with the increase of the diradical character. As seen from Figure 3 and Table 1, the deviations of TDA-UY results from the UCCSD and UCCSD(T) results tend to decrease with the increase of the diradical character. Among the four types of TDA-UY (Y = BLYP, B3LYP, BHandHLYP, and HFLYP) methods, the TDA-UBHandHLYP method is found to give the most reliable values: 121%, 103%, 113%, and 113% of UCCSD(T) results for system **1**, **2**, **3**, and **4**, respectively. Thus, the inclusion of appropriate fraction of HF exchange in the xc-functional turns out to be essential for the semiquantitative description of static and off-resonant α values. It is also noted that the BHandHLYP functional is also appropriate for the semiquantitative description of the diradical character dependence of the second hyperpolarizability of open-shell singlet systems.[14a−d,16]

The frequency dispersion of α is known to strongly depend on the peak position (excitation energy) and intensity (related to transition amplitude). Table 2 summarizes the positions of the primary peaks and the corresponding transition moment amplitudes for these systems calculated by the TDA-UY methods. We compare these results with the spin-unrestricted equation-of-motion (EOM)-UCCSD results, which are known to give reliable excitation energies and transition moments. The peak positions of systems **1**−**4** calculated by the EOM-UCCSD method are shown to be reproduced well by the TDA-UBH andHLYP method: the maximum relative error of the TDA-UBHandHLYP peak position, which is observed in system **2**, is less than 8%, and even for system **4**, exhibiting the largest xc-functional dependence of the peak position among these TDA-UDFT results (see Figure 2), the relative error of the TDA-UBHandHLYP peak position is less than 4%. Furthermore, the transition moment amplitude, which relates to the peak intensity, is also well described by the TDA-UBHandHLYP (with an average error ∼15% relative to the EOM-UCCSD results) compared to the other xc-functionals. It is also noted that the diradical character dependences of the first excitation energies and transition moment amplitudes are in qualitative agreement with those by the valence configuration interaction method with two-site model[14e,15l,17] though the present results are obtained by different molecules. It is indeed found that as increasing the diradical character y, the transition moment amplitude decreases, while the first excitation energy first decreases (see **1**−**3**) and then increases (see **4**). The former behavior is explained by the relative increase of diradical component in the ground state in contrast to the constant ionic component in the first excited state, as increasing the diradical character y, while the latter behavior is understood by the facts that the first excitation energy (E_1) divided by the effective Coulomb repulsion (U), E_1/U, rapidly decreases with increasing y in the relatively small y region and asymptotically approaches to 1 in the large y region, while that U monotonically increases with increasing y.[14e,15l,17]

Because the highly computational demand of the EOM-UCCSD calculations limits the number of excited states obtained, we cannot directly compare the EOM-UCCSD dynamic polarizability with the BS-TDA-DFTQME results. However, judging from the results of α in the static limit condition at the UCCSD and

Table 1. Static Polarizabilities α (≡ α_{zz}) [a.u.] of Systems 1-4 Calculated by the Finite-Field Method Based on the UCCSD and UCCSD(T) Levels of Approximation Using the 6-31G Basis Set As Well As the Diradical Character, y [-], Calculated from the Occupation Numbers of Natural Orbitals Obtained by the UHF/6-31G** Method**

system	1	2	3	4
y	0.15	0.35	0.59	0.91
α [UCCSD]	61.3	48.6	40.8	34.3
α [UCCSD(T)]	61.7	52.0	40.9	34.6

Table 2. Primary Peak Positions ω_1 [cm^{-1}] and the Corresponding Amplitudes of Transition Dipole Moments $|\mu|$ [D] for Systems 1-4 Calculated by the TDA-UY (Y = BLYP, B3LYP, BHandHLYP, and HFLYP) and the EOM-UCCSD Methods

	1		2		3		4	
	ω_1 [cm^{-1}]	$\lvert\mu\rvert$ [D]	ω_1 [cm^{-1}]	$\lvert\mu\rvert$ [D]	ω_1 [cm^{-1}]	$\lvert\mu\rvert$ [D]	ω_1 [cm^{-1}]	$\lvert\mu\rvert$ [D]
TDA-UBLYP	52598	6.04	49047	5.90	15456	1.86	18371	1.26
TDA-UB3LYP	50670	6.13	42237	5.19	18924	1.74	26309	0.95
TDA-UBHandHLYP	46155	5.54	41273	3.99	24226	1.52	38903	0.71
TDA-UHFLYP	46893	4.43	50848	3.08	31158	1.19	57917	0.52
EOM-UCCSD	43035	5.01	40051	4.01	22797	1.18	40415	0.59

dx.doi.org/10.1021/jp200056m |*J. Phys. Chem. A* 2011, 115, 3565–3575

UCCSD(T) levels, the BS-DFTQME method combined with the TDA-UBHandHLYP calculations is expected to give the reliable off-resonant α values as well as their frequency dispersions (up to the first main peaks) of the present 1,3-dipole molecules.

4. CONCLUSIONS

We have developed a novel method, referred to as BS-DFTQME, for the electron dynamics of open-shell molecular systems based on the BS-TD(U)DFT method within the TDA. We present the dynamic representation of electron, hole, and spin density distributions defined from the α- and β-electron contributions to the polarization density together with a method for calculation and analysis of dynamic polarizability and its density, which can be partitioned into the contribution of each orbital pair. The application of this method to the calculation of polarizabilities of simple π-conjugated open-shell systems, 1,3-dipoles, having different diradical characters has elucidated that the frequency dispersion of polarizability exhibits strong xc-functional dependence, in particular, in the large diradical character region. It turns out that the inclusion of HF exchange in the xc-functional plays an important role for the qualitative and semiquantitative descriptions of frequency dispersion of polarizability, where the frontier orbital contribution is enhanced significantly. It is found that the off-resonant α values tend to decrease with the increase of diradical character for these 1,3-dipoles.

Within the present systems, the BS-DFTQME method using the TDA-UBHandHLYP results is expected to semiquantitatively reproduce the polarizability calculated at the EOM-UCCSD level of approximation in the off-resonant region. This predicts the importance of including the fraction of HF exchange for calculating the excitation energies and transition properties of lower-lying excited states of open-shell systems though further investigation is necessary for the confirmation.

The advantages of the present method exist in providing a nonperturbative method for calculation of the static and dynamic response properties as well as for analysis of the electron−hole and/or spin polarization dynamics for such properties of open-shell molecular systems. The BS-DFTQME method is indeed expected to be straightforwardly applied to the evaluation of dynamic nonlinear optical responses of open-shell systems. Furthermore, an intriguing extension of this method is to combine with a recently proposed dynamic description of open-shell character together with a partition scheme of response properties to natural orbital contributions.[32] Such studies will shed light on the role of open-shell character and odd electrons on the unexplored electron dynamics in open-shell molecular chemistry.

AUTHOR INFORMATION

Corresponding Author

*Fax: +81 668506268. E-mail: rkishi@cheng.es.osaka-u.ac.jp (R.K.), mnaka@cheng.es.osaka-u.ac.jp (M.N.).

ACKNOWLEDGMENT

This work is supported by Grant-in-Aid for Scientific Research (Nos. 21350011 and 20655003) and "Japan-Belgium Cooperative Program" from Japan Society for the Promotion of Science (JSPS), Grant-in-Aid for Scientific Research on Priority Areas (No. 18066010) from the Ministry of Education, Culture, Sports, Science and Technology (MEXT), and the global COE (center of excellence) program "Global Education and Research Center for Bio-Environmental Chemistry" of Osaka University. Theoretical calculations for the QME dynamics were partly performed using Research Center for Computational Science, Okazaki, Japan. The isosurfaces of polarizability densities are visualized using the VMD (visual molecular dynamics) program package.[31]

REFERENCES

(1) (a) Salem, L.; Ronland, C. *Angew. Chem., Int. Ed.* **1972**, *11*, 92. (b) Döhnert, D.; Koutecký, J. *J. Am. Chem. Soc.* **1980**, *102*, 1789.(c) *Diradicals*, Borden, W. T., Ed.;Wiley-Interscience: New York, 1982. (d) Rajca, A. *Chem. Rev.* **1994**, *94*, 871.

(2) (a) Borden, W. T.; Davidson, E. R. *J. Am. Chem. Soc.* **1977**, *99*, 4587. (b) Staroverov, V. N.; Davidson, E. R. *J. Am. Chem. Soc.* **2000**, *122*, 186. (c) Abe, M.; Adam, W.; Hara, M.; Hattori, M.; Majima, T.; Nojima, M.; Tachibana, K.; Tojo, S. *J. Am. Chem. Soc.* **2002**, *124*, 6540. (d) Jung, Y.; Head-Gordon, M. *Chem. Phys. Chem.* **2003**, *4*, 522.

(3) Paci, I.; Johnson, J. C.; Chen, X.; Rana, G.; Popovic, D.; David, D. E.; Nozik, A. J.; Ratner, M. A.; Michl, J. *J. Am. Chem. Soc.* **2006**, *128*, 16546.

(4) Suaud, N.; Bonnet, M. L.; Boilleau, C.; Labéguerie, P.; Guihéry, N. *J. Am. Chem. Soc.* **2009**, *131*, 715.

(5) (a) Scheschkewitz, D.; Amii, H.; Gomitzka, H.; Schoeller, W. W.; Bourissou, D.; Bertrand, G. *Science* **2002**, *295*, 1880. (b) Cui, C.; Brynda, M.; Olmstead, M. M.; Power, P. P. *J. Am. Chem. Soc.* **2004**, *126*, 6510.

(6) Bachler, V.; Olbrich, G.; Neese, F.; Wieghardt, K. *Inorg. Chem.* **2002**, *41*, 4179.

(7) Motta, S. D.; Negri, F.; Fazzi, D.; Castiglioni, C.; Canesi, E. V. *J. Phys. Chem. Lett.* **2010**, *1*, 3334.

(8) Kikuchi, A.; Iwahori, F.; Abe, J. *J. Am. Chem. Soc.* **2004**, *126*, 6526.

(9) (a) Houk, K. N.; Lee, P. S.; Nendel, M. *J. Org. Chem.* **2001**, *66*, 5517. (b) Bendikov, M.; Duong, H. M.; Starkey, K.; Houk, K. N.; Carter, E. A.; Wudl, F. *J. Am. Chem. Soc.* **2004**, *126*, 7416. (c) Chen, Z.; Jiang, D.; Lu, X.; Bettinger, H. F.; Dai, S.; Schleyer, P. v. R.; Houk, K. N. *Org. Lett.* **2007**, *9*, 5449. (d) Hachmann, J.; Dorando, J. J.; Avilés, M.; Chan, G. K.-L. *J. Chem. Phys.* **2007**, *127*, 134309. (e) Jiang, D.; Dai, S. *J. Phys. Chem. A* **2008**, *112*, 332. (f) Qu, Z.; Zhang, D.; Liu, C.; Jiang, Y. *J. Phys. Chem. A* **2009**, *113*, 7909. (g) Tönshoff, C.; Bettinger, H. F. *Angew. Chem., Int. Ed.* **2010**, *49*, 4125. (h) Zade, S. S.; Bendikov, M. *Angew. Chem., Int. Ed.* **2010**, *49*, 4012.

(10) (a) Wassmann, T.; Seitsonen, A. P.; Saitta, A. M.; Lazzeri, M.; Mauri, F. *J. Am. Chem. Soc.* **2010**, *132*, 3440. (b) Nagai, H.; Nakano, M.; Yoneda, K.; Kishi, R.; Takahashi, H.; Shimizu, A.; Kubo, T.; Kamada, K.; Ohta, K.; Botek, E.; Champagne, B. *Chem. Phys. Lett.* **2010**, *489*, 212. (c) Trinquier, G.; Suaud, N.; Malrieu, J. P. *Chem.—Eur. J.* **2010**, *16*, 8762. (d) Wang, W. L.; Meng, S.; Kaxiras, E. *Nano Lett.* **2008**, *8*, 241. (e) Yazyev, O. V.; Wang, W. L.; Meng, S.; Kaxiras, E. *Nano Lett.* **2008**, *8*, 766. (f) Ezawa, M. *Phys. Rev. B* **2007**, *76*, 245415. (g) Vandeschuren, M.; Hermet, P.; Meunier, V.; Henrard., L.; Lambin., Ph. *Phys. Rev. B* **2008**, *78*, 195401. (h) F-Rossier, J.; Palacios, J. J. *Phys. Rev. Lett.* **2007**, *99*, 177204. (i) Dias, J. R. *Chem. Phys. Lett.* **2008**, *467*, 200. (j) Son, Y.-W.; Cohen, M. L.; Louie, S. G. *Nature* **2006**, *444*, 347. (k) Goto, K.; Kubo, T.; Yamamoto, K.; Nakasuji, K.; Sato, K.; Shiomi, D.; Takui, T.; Kubota, M.; Kobayashi, T.; Yakushi, K.; Ouyang, J. *J. Am. Chem. Soc.* **1999**, *121*, 1619. (l) Takano, Y.; Taniguchi, T.; Isobe, H.; Kubo, T.; Morita, Y.; Yamamoto, K.; Nakasuji, K.; Takui, T.; Yamaguchi, K. *J. Am. Chem. Soc.* **2002**, *124*, 11122. (m) Kubo, T.; Shimizu, A.; Sakamoto, M.; Uruichi, M.; Yakushi, K.; Nakano, M.; Shiomi, D.; Sato, K.; Takui, T.; Morita, Y.; Nakasuji, K. *Angew. Chem., Int. Ed.* **2005**, *44*, 6564. (n) Konishi, A.; Hirao, Y.; Nakano, M.; Shimizu, A.; Botek, E.; Champagne, B.; Shiomi, D.; Sato, K.; Takui, T.; Matsumoto, K.; Kurata, H.; Kubo, T. *J. Am. Chem. Soc.* **2010**, *132*, 11021. (o) Umeda, R.; Hibi, D.; Miki, K.; Tobe, Y. *Org. Lett.* **2009**, *11*, 4104.

(11) (a) Lahti, P. M.; Ichimura, A. S.; Sanborn, J. A. *J. Phys. Chem. A* **2001**, *105*, 251. (b) Serwinski, P. R.; Lahti, P. M. *Org. Lett.* **2003**, *5*, 2099. (c) Ito, A.; Urabe, M.; Tanaka, K. *Angew. Chem., Int. Ed.* **2007**, *46*, 3300. (d) Matsuda, K.; Irie, M. *Chem.—Eur. J.* **2001**, *7*, 3466. (e) Rajca, A.; Shiraishi, K.; Pink, M.; Rajca, S. *J. Am. Chem. Soc.* **2007**, *129*, 7232. (f) Rajca, A.; Vale, M.; Rajca, S. *J. Am. Chem. Soc.* **2008**, *130*, 9099. (g) Train, C.; Norel, L.; Baumgarten, M. *Coord. Chem. Rev.* **2009**, *253*, 2342.

(12) Shimizu, A.; Uruichi, M.; Yakushi, K.; Matsuzaki, H.; Okamoto, H.; Nakano, M.; Hirao, Y.; Matsumoto, K.; Kurata, H.; Kubo, T. *Angew. Chem., Int. Ed.* **2009**, *48*, 5482.

(13) (a) Huang, J.; Kertesz, M. *J. Am. Chem. Soc.* **2007**, *129*, 1634. (b) Tian, Y. H.; Kertesz, M. *J. Am. Chem. Soc.* **2010**, *132*, 10648.

(14) (a) Nakano, M.; Nitta, T.; Yamaguchi, K.; Champagne, B.; Botek, E. *J. Phys. Chem. A* **2004**, *108*, 4105. (b) Nakano, M.; Kishi, R.; Nitta, T.; Kubo, T.; Nakasuji, K.; Kamada, K.; Ohta, K.; Champagne, B.; Botek, E.; Yamaguchi, K. *J. Phys. Chem. A* **2005**, *109*, 885. (c) Nakano, M.; Kubo, T.; Kamada, K.; Ohta, K.; Kishi, R.; Ohta, S.; Nakagawa, N.; Takahashi, H.; Furukawa, S.; Morita, Y.; Nakasuji, K.; Yamaguchi, K. *Chem. Phys. Lett.* **2006**, *418*, 142. (d) Nakano, M.; Kishi, R.; Ohta, S.; Takebe, A.; Takahashi, H.; Furukawa, S.; Kubo, T.; Morita, Y.; Nakasuji, K.; Yamaguchi, K.; Kamada, K.; Ohta, K.; Champagne, B.; Botek, E. *J. Chem. Phys.* **2006**, *125*, 074113. (e) Nakano, M.; Kishi; Ohta, S.; Takahashi, H.; Kubo, T.; Kamada, K.; Ohta, K.; Botek, E.; Champagne, B. *Phys. Rev. Lett.* **2007**, *99*, 033001. (f) Nakano, M.; Champagne, B.; Botek, E.; Ohta, K.; Kamada, K.; Kubo, T. *J. Chem. Phys.* **2010**, *133*, 154302.

(15) (a) Kamada, K.; Ohta, K.; Kubo, T.; Shimizu, A.; Morita, Y.; Nakasuji, K.; Kishi, R.; Ohta, S.; Furukawa, S.; Takahashi, H.; Nakano, M. *Angew. Chem., Int. Ed.* **2007**, *46*, 3544. (b) Hu, W.; Ma, H.; Liu, C.; Jiang, Y. *J. Chem. Phys.* **2007**, *126*, 044903. (c) Yesudas, K.; Bhanuprakash, K. *J. Phys. Chem. A* **2007**, *111*, 1943. (d) Srinivas, K.; Prabhakar, Ch.; Devi, C. L.; Yesudas, K.; Bhanuprakash, K.; Rao, V. J. *J. Phys. Chem. A* **2007**, *111*, 3378. (e) Thomas, A.; Srinivas, K.; Prabhakar, Ch.; Bhanuprakash, K.; Rao, V. J. *Chem. Phys. Lett.* **2008**, *454*, 36. (f) Qiu, Y. Q.; Fan, H. L.; Sun, S. L.; Liu, C. G.; Su, Z. M. *J. Phys. Chem. A* **2008**, *112*, 83. (g) Li, Z. J.; Wang, F. F.; Li, Z. R.; Xu, H. L.; Huang, X. R.; Wu, D.; Chen, W.; Yu, G. T.; Gu, F. L.; Aoki, Y. *Phys. Chem. Chem. Phys.* **2009**, *11*, 402. (h) Jha, P. C.; Rinkevicius, Z.; Ågren, H. *ChemPhysChem* **2009**, *10*, 817. (i) Serrano-Andrés, L.; Avramopoulos, A.; Li, J.; Labéguerie, P.; Bégué, D.; Kellö, V.; Papadopoulos, M. G. J. *Chem. Phys.* **2009**, *131*, 134312. (j) Kishida, H.; Hibino, K.; Nakamura, A.; Kato, D.; Abe, J. *Thin Solid Films* **2010**, *519*, 1028. (k) Umeda, R.; Hibi, D.; Miki, K.; Tobe, Y. *Pure Appl. Chem.* **2010**, *82*, 871. (l) Kamada, K.; Ohta, K.; Shimizu, A.; Kubo, T.; Kishi, R.; Takahashi, H.; Botek, E.; Champagne, B.; Nakano, M. *J. Phys. Chem. Lett.* **2010**, *1*, 937.

(16) (a) Nakano, M.; Kishi, R.; Nakagawa, N.; Ohta, S.; Takahashi, H.; Furukawa, S.; Kamada, K.; Ohta, K.; Champagne, B.; Botek, E.; Yamada, S.; Yamaguchi, K. *J. Phys. Chem. A* **2006**, *110*, 4238. (b) Ohta, S.; Nakano, M.; Kubo, T.; Kamada, K.; Ohta, K.; Kishi, R.; Nakagawa, N.; Champagne, B.; Botek, E.; Takebe, A.; Umezaki, S.; Nate, M.; Takahashi, H.; Furukawa, S.; Morita, Y.; Nakasuji, K.; Yamaguchi, K. *J. Phys. Chem. A* **2007**, *111*, 3633. (c) Kishi, R.; Nakano, M.; Ohta, S.; Takebe, A.; Nate, M.; Takahashi, H.; Kubo, T.; Kamada, K.; Ohta, K.; Botek, E.; Champagne, B. *J. Chem. Theory Comput.* **2007**, *3*, 1699. (d) Nakano, M.; Ohta, S.; Tokushima, K.; Kishi, R.; Kubo, T.; Kamada, K.; Ohta, K.; Champagne, B.; Botek, E.; Takahashi, H. *Chem. Phys. Lett.* **2007**, *443*, 95. (e) Fukui, H; Kishi, R.; Minami, T.; Nagai, H.; Takahashi, H.; Kubo, T.; Kamada, K.; Ohta, K.; Champagne, B.; Botek, E.; Nakano, M. *J. Phys. Chem. A* **2008**, *112*, 8423. (f) Nakano, M.; Nagai, H.; Fukui, H.; Yoneda, K.; Kishi, R.; Takahashi, H.; Shimizu, A.; Kubo, T.; Kamada, K.; Ohta, K.; Champagne, B.; Botek, E. *Chem. Phys. Lett.* **2008**, *467*, 120. (g) Kishi, R.; Bonness, S.; Yoneda, K.; Takahashi, H.; Nakano, M.; Botek, E.; Champagne, B.; Kubo, T.; Kamada, K.; Ohta, K.; Tsuneda, T. *J. Chem. Phys.* **2010**, *132*, 094107. (h) Bonness, S.; Fukui, H.; Yoneda, K.; Kishi, R.; Champagne, B.; Botek, E.; Nakano, M. *J. Chem. Phys.* **2010**, *132*, 094107. (i) Nakano, M.; Minami, T.; Fukui, H.; Yoneda, K.; Shigeta, Y.; Kishi, R.; Champagne, B.; Botek, E. *Chem. Phys. Lett.* **2010**, *501*, 140.

(17) (a) Nakano, M.; Yoneda, K.; Kishi, R.; Takahashi, H.; Kubo, T.; Kamada, K.; Ohta, K.; Botek, E.; Champagne, B. *J. Chem. Phys.* **2009**, *131*, 114316.(b) Nakano, M.; Yoneda, K.; Kishi, R.; Takahashi, H.; Kubo, T.; Kamada, K.; Ohta, K.; Champagne, B.; Botek, E. *AIP conference proceedings (ICCMSE 2009)*, in press.

(18) (a) Orr, B. J.; Ward, J. F. *Mol. Phys.* **1971**, *20*, 513. (b) Bishop, D. M. *J. Chem. Phys.* **1994**, *100*, 6535. (c) Nakano, M.; Okumura, M.; Yamaguchi, K.; Fueno, T. *Mol. Cryst. Liq. Cryst.* **1989**, *182*, A 1.

(19) (a) Luo, Y.; Ågren, H.; Jørgensen, P.; Mikkelsen, K. V. *Adv. Quantum Chem.* **1995**, *26*, 165. (b) Sekino, H.; Bartlett, R. J. *J. Chem. Phys.* **1986**, *85*, 976. (c) Karna, S. P.; Dupuis, M. *J. Comput. Chem.* **1991**, *12*, 487. (d) Sekino, H.; Bartlett, R. J. *J. Chem. Phys.* **1991**, *94*, 3665. (e) Norman, P.; Jonsson, D.; Vahtras, O.; Ågren, H. *Chem. Phys. Lett.* **1995**, *242*, 7.

(20) (a) Sasagane, K.; Aiga, F.; Itoh, R. *J. Chem. Phys.* **1993**, *98*, 3022. (b) Kobayashi, T.; Sasagane, K.; Aiga, F.; Yamaguchi, K. *J. Chem. Phys.* **1999**, *111*, 842. (c) Aiga, F.; Tada, T.; Yoshimura, R. *J. Chem. Phys.* **1999**, *111*, 2878.

(21) (a) Ho, T.-S.; Wang, K.; Chu, S.-I. *Phys. Rev. A* **1985**, *33*, 1798. (b) Wang, K.; Chu, S.-I. *J. Chem. Phys.* **1986**, *86*, 3225.

(22) (a) Nakano, M.; Yamaguchi, K. *Phys. Rev. A* **1994**, *50*, 2989. (b) Nakano, M.; Yamaguchi, K.; Matsuzaki, Y.; Tanaka, K.; Yamabe, T. *J. Chem. Phys.* **1995**, *102* (2986), 2996. (c) Nakano, M.; Yamaguchi, K. *Chem. Phys. Lett.* **1995**, *234*, 323.

(23) (a) Nakano, M.; Takahata, M.; Yamada, S.; Kishi, R.; Nitta, T.; Yamaguchi, K. *J. Chem. Phys.* **2004**, *120*, 2359. (b) Nakano, M.; Kishi, R.; Minami, T.; Fukui, H.; Nagai, H.; Yoneda, K.; Takahashi, H. *Chem. Phys. Lett.* **2008**, *460*, 370. (c) Kishi, R.; Nakano, M.; Minami, T.; Fukui, H.; Nagai, H.; Yoneda, K.; Takahashi, H. *J. Phys. Chem. A* **2009**, *113*, 5455. (d) Kishi, R.; Nakano, M.; Minami, R.; Fukui, H.; Nagai, H.; Yoneda, K.; Takahashi, H. *Synth. Met.* **2009**, *159*, 2194.(e) Kishi, R.; Minami, T.; Yoneda, K.; Nakano, M. *AIP conference proceedings (ICCMSE 2009)*, in press. (f) Kishi, R.; Minami, T.; Fukui, H.; Takahashi, H.; Nakano, M. *J. Chem. Phys.* **2008**, *128*, 244306. (g) Nakano, M.; Kishi, R.; Minami, M.; Yoneda, K. *Molecules* **2009**, *14*, 3700.

(24) (a) Tamm, I. *J. Phys. (USSR)* **1945**, *9*, 449. (b) Dancoff, S. M. *Phys. Rev.* **1950**, *78*, 382. (c) Hirata, S.; Head-Gordon, M. *Chem. Phys. Lett.* **1999**, *314*, 291.

(25) Nakano, M.; Yamada, S.; Shigemoto, I.; Yamaguchi, K. *Chem. Phys. Lett.* **1996**, *250*, 247.

(26) (a) Hayes, E. F.; Siu, A. K. Q. *J. Am. Chem. Soc.* **1971**, *93*, 2090. (b) Yamaguchi, K. *Chem. Phys. Lett.* **1975**, *33*, 330.(c) Yamaguchi, K. In *Self-Consistent Field Theory and Applications*; Carbo, R., Klobukowski, M., Eds.; Elsevier: Amsterdam, 1990; p 727.

(27) (a) Nakano, M.; Takahata, M.; Fujita, H.; Kiribayashi, S.; Yamaguchi, K. *Chem. Phys. Lett.* **2000**, *323*, 249. (b) Takahata, M.; Nakano, M.; Fujita, H.; Yamaguchi, K. *Chem. Phys. Lett.* **2002**, *363*, 422. (c) Ohta, S.; Nakano, M.; Kishi, R.; Takahashi, H.; Furukawa, S.-i. *Chem. Phys. Lett.* **2006**, *419*, 70. (d) Nakano, M.; Kishi, R.; Nakagawa, N.; Nitta, T.; Yamaguchi, K. *J. Phys. Chem. B* **2005**, *109*, 7631. (e) Takahata, M.; Shoji, M.; Nitta, H.; Takeda, R.; Yamanaka, S.; Okumura, M.; Nakano, M.; Yamaguchi, K. *Int. J. Quantum Chem.* **2005**, *105*, 615.

(28) (a) Carmichael, H. J. *Statistical Methods in Quantum Optics 1*; Springer, Verlag: Berlin, 1999. (b) Leegwater, J. A.; Durrant, J. R.; Klug, D. R. *J. Phys. Chem. B* **1997**, *101*, 7205.

(29) Nakano, M.; Kishi, R.; Fukui, H.; Minami, T.; Nagai, H.; Yoneda, K.; Bonness, S.; Takahashi, H. *Int. J. Nanosci.* **2009**, *8*, 123.

(30) (a) Straatsma, T. P.; Aprà, E.; Windus, T. L.; Bylaska, E. J.; de Jong, W.; Hirata, S.; Valiev, M.; Hackler, M.; Pollack, L.; Harrison, R.; Dupuis, M.; Smith, D. M. A.; Nieplocha, J.; Tipparaju, V.; Krishnan, M.; Auer, A. A.; Brown, E.; Cisneros, G.; Fann, G.; Früchtl, H.; Garza, J.; Hirao, K.; Kendall, R.; Nichols, J.; Tsemekhman, K.; Wolinski, K.; Anchell, J.; Bernholdt, D.; Borowski, P.; Clark, T.; Clerc, D.; Dachsel, H.; Deegan, M.; Dyall, K.; Elwood, D.; Glendening, E.; Gutowski, M.; Hess, A.; Jaffe, J.; Johnson, B.; Ju, J.; Kobayashi, R.; Kutteh, R.; Lin, Z.; Littlefield, R.; Long, X.; Meng, B.; Nakajima, T.; Niu, S.; Rosing, M.; Sandrone, G.; Stave, M.; Taylor, H.; Thomas, G.; van Lenthe, J.; Wong, A.; Zhang, Z. *NWChem, A Computational Chemistry Package for Parallel*

Computers, Version 4.6, Pacific Northwest National Laboratory: Richland, Washington 99352-0999, USA, 2004. (b) Kendall, R. A.; Aprà, E.; Bernholdt, D. E.; Bylaska, E. J.; Dupuis, M.; Fann, G. I.; Harrison, R. J.; Ju, J.; Nichols, J. A.; Nieplocha, J.; Straatsma, T. P.; Windus, T. L.; Wong, A. T. *Comput. Phys. Commun.* **2000**, *128*, 260.

(31) Humphrey, W.; Dalke, A.; Schulten, K. *J. Mol. Graphics* **1996**, *14*, 33.

(32) Nakano, M.; Fukui, H., Minami, T.; Yoneda, K.; Shigeta, Y.; Kishi, R.; Champagne, B.; Botek, E.; Kubo, T.; Ohta, K.; Kamada, K. *Theor. Chem. Acc.*, DOI 10.1007/s00214-010-0871-y.